Combustion Processes in Supersonic Flow

Frederick S. Billig*
The Johns Hopkins University, Laurel, Maryland

Three general classes of models that describe the processes occurring in diabatic flow in ducts having supersonic entry conditions are discussed. They are: integral techniques, finite-difference methods, and exact two-dimensional planar flame models formulated on the basis of instantaneous heat release. All three methods rigorously satisfy the conservation equations. The first two methods provide a basis for predicting and analyzing supersonic combustor performance. The careful interpretation and judicious use of experimental observations are crucial for the successful application of these methods. Comparisons of analytical and experimental results are presented, and generalized parametric studies are included. The third method is based on an idealized mixing and combustion model that may not be achievable, but nonetheless serves as a valuable analytical tool for explaining complex processes involving shock waves and heat addition. Results from four types of flow structures are discussed.

Nomenclature

A = cross-sectional area
A_i = projected area of inlet
A_w = wall area
A_x = projected area in axial direction
C_f = skin-friction coefficient
h = enthalpy
M = Mach number
p = pressure
q = dynamic pressure
Q_w = wall heat flux
r = radius
S_d = distance shock train extends into combustor (Fig. 1)
S_s = length of the shock train (Fig. 1)
T = temperature
u = velocity
x = axial distance (Fig. 1)
z = altitude
β = fuel injection angle
γ = ratio of specific heats
δ = OPH turning angle (Fig. 10)
δ_w = shock-turning angle
ε = constant in pressure area relationship [Eq. (1)]
η_c = combustion efficiency
η_{KE} = inlet kinetic energy efficiency
θ = OPH heater angle (Fig. 10)
θ_w = shock angle
ρ = density
τ_w = wall shearing stress

Subscripts

b = conditions at exit of fuel injector
e = conditions at upstream end of 1D approach zone (Fig. 1)
f^* = throat conditions in fuel injector (Fig. 1)
g = conditions at point of separation in fuel injector (Fig. 1)
s = conditions at downstream end of shock train (Fig. 1)
t = total
0 = freestream
1 = conditions upstream of OPH
2 = conditions downstream of OPH
4 = combustor entrance
5 = combustor exit

Received Jan. 24, 1986; revision received May 14, 1987.

*Chief Scientist, Applied Physics Laboratory; Associate Department Head, Aeronautics Department.

Introduction

THE literature is abundant with discussions of techniques to analyze supersonic flows with heat addition. They vary in complexity from simple one-dimensional constant area or constant pressure processes (e.g., Ref. 1) to complex time-dependent solutions of the Navier-Stokes equations, including finite-rate chemistry (e.g., Ref. 2). The former are generally deficient because they neglect physical processes that lead to first-order effects on the results, and the latter require enormous computational resources that are excessive for design and development efforts. Consequently, it is prudent to explore the potential of techniques that include modeling based on experimental results that can adequately describe the flowfield but substantially reduce the computational effort. In particular, if the effects of localized separated zones on the main flow can be assessed without a rigorous solution of the flow within the zones, then forward-marching instead of time-dependent solutions can be made. Computational times can thereby be reduced by one to two orders of magnitude. The first section of the present paper presents a method that meets this objective.

For more than 40 years, (e.g., Refs. 3 and 4) simplified exact solutions for diabatic flows have been sought that could aid in the understanding of the effects of heat release in compressible flow. In Ref. 5, the concept of the oblique planar heater, an exact solution for two-dimensional inviscid flow with heat release was introduced to help to describe the concept of thermal compression that had been proposed by Ferri.[6] The last section of the paper extends the modeling of Ref. 5 to provide direct comparisons with results from the integral solutions.

Models for Integral and Finite-Difference Solutions

Figure 1 shows the general features of the flowfields upon which development of the integral and finite-difference models are based. Gaseous fuel is injected at either sonic or supersonic conditions at angle β into a supersonic airstream. The blockage due to combined effects of the injection and heat release generates a "shock train" disturbance which, in general, originates upstream of the fuel injector ports and extends into the combustor. At moderate combustor inlet Mach numbers M_4, i.e., 1.5–4, and typical fuel-air equivalence ratios, i.e., 0.5–1.0, the pressure rise associated with the shock train is of sufficient strength to separate the incoming boundary layer. In a well-designed engine, an isolator is placed between combustor and air inlet to prevent the combustion-induced disturbances from disrupting the flow in the inlet. The length of the shock train is defined as the length of the corresponding s-shaped pressure rise and is given as S_s. The distance that the shock train extends into the combustor is S_d. Empirical relationships for S_s and S_d have been obtained from correlations of experimental data that

will be summarized herein. As flight speed increases, M_4 correspondingly increases and the strength of the pressure rise in the shock train decreases and the separated zone may not be present.

Downstream of the shock train, mixing and combustion are intensive, with large radial, axial, and perhaps circumferential gradients in flow properties and chemical composition. This region extends from station s to station e and i labeled "two- or three-dimensional mixing and combustion zone." Further downstream, the mixing and combustion are less intense, and the gradients are considerably weaker. This region extends from station e to station 5 and is labeled "one-dimensional approach zone." In the integral models, the flow in this region is approximated by one-dimensional mean-flow properties at each axial station. At this stage in development of the finite-difference models, circumferential symmetry is assumed and, therefore, regions s to e and e to 5 are indistinguishable. Radial gradients in flow properties and composition are typical but, in general, the gradients decrease as the combustor exit is approached. The control boundary that forms the basis for the integral models comprises the plane at station 4 upstream of the shock train, the throat of the injector, the injector and combustor walls, and the combustor exit plane at station 5. Flow properties on the end planes need not be constant, but to simplify the discussion that follows, representative mean values of ρ, u, p, h, and T are taken at stations 4 and 5 together with the respective geometric duct areas. For more rigorous analyses when gradients are present, mass-averaged values are used in conjunction with a suitably defined area that simultaneously satisfies continuity, energy and mass-averaged total pressure.[7]

When used independently, both the integral and finite-difference methods for solution have deficiencies. However, if the techniques are coupled by a unique procedure, these deficiencies can be virtually eliminated. The general features of this approach are shown in Fig. 2. The first step is to solve the integral equations for given initial conditions and combustor geometry to obtain the axial pressure distribution $p(x)$ with modeled values for wall shear τ_w, and heat transfer Q_w, and an assumed value for the combustion efficiency η_c. Modeling of the pressure distribution in the shock train, and on the base, together with the $\varepsilon = C$ pressure-area distribution discussed below in the one-dimensional approach zone, is inherent in the entire method. With $p(x)$ so defined, a simplified finite-difference calculation that avoids calculating flow in the separated regions is made to obtain τ_w, Q_w, and η_c analytically. Inherent to the finite-difference method are models for kinetic rates and turbulent mixing. The integral solution is then repeated using these values of τ_w, Q_w, and η_c to obtain a new $p(x)$ and so forth. The iteration ends when the flow area $A(x)$, obtained from the finite-difference solution, agrees with the geometric area downstream of station s.

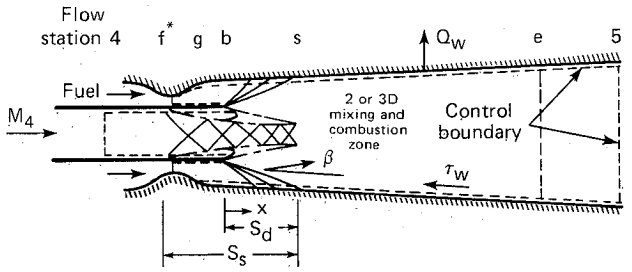

Fig. 1 Flow processes in combustor with supersonic diffusive flames.

In principle, a finite-difference solution could be obtained using the geometric $A(x)$, and thereby avoid depending on $p(x)$ from the integral method. In practice, the presence of the separated zone would have to be accurately calculated, and the simplifying assumptions that permit the use of the boundary layer or parabolized forms of the Navier-Stokes equations could not be made. The form of the conservation equations would be elliptic and solutions would have to be obtained using time-dependent techniques. References 2 and 9 describe routines for such techniques that require hours of CPU time on the largest computers. Given the uncertainties that still remain in adequately describing kinetic processes, their associated rate constants, the transport properties, and the models for turbulence, the simpler, far less expensive approach has considerable merit.

At present, solutions have been obtained that were based on the assumption that radial and circumferential pressure gradients are negligible, thereby permitting use of the boundary layer form of the conservation equations. Additionally, it is more expeditious to first solve for the inviscid "core" flow in the combustor, iterate for $p(x)$, and then solve for the boundary layer using edge conditions from the core flow and a dense grid point spacing in the radial direction. Details of the modeling and calculational procedures are given in Refs. 10 and 11.

Typical results from Ref. 10 for the combustion of Shelldyne H fuel at equivalence ratio of 0.5 are shown in Fig. 3. The shape of the double flame sheets and the computed $A(x)$ are shown for two combustor-entry conditions corresponding to flight at Mach 4 at 37,000 ft and Mach 7 at 61,000 ft. Flame sheets as contrasted to diffusive reaction zones are the result of simplifying assumptions for kinetic rates in this exemplary case. The computed $A(x)$ distributions in this dual-combustor ramjet show that the separated zones extend into about 20% of the combustor at both conditions.

The derived flow properties in the combustor-exit plane provide initial conditions for a subsequent calculation of the flow in the expansion nozzle. Note, however, that station 5 has been somewhat arbitrarily defined in the case where a nozzle is attached. To remove this ambiguity, a further step in the iterative procedure is to redefine station 5 based on the condition $dT_t/T_t \to 0$, which is determined from the finite-difference solution.

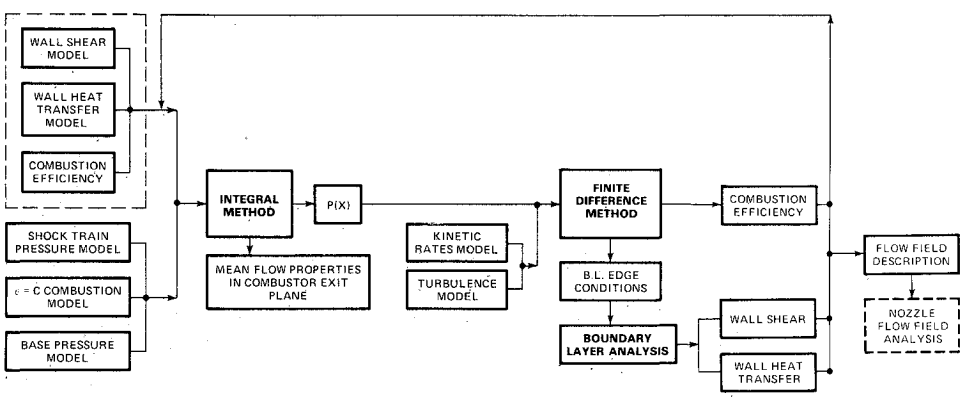

Fig. 2 Method of computation for supersonic combustion analysis.

Use of the Integral Method for Design and Analysis

Whereas the sophistication of the coupled approach is required to yield an adequate description of the flow in the combustor, there is considerable merit in using the integral method independently to 1) assess experimental data when sufficient measurements have been made to enable comparisons with theory; 2) develop an understanding of the key interactive features of the flow, viz., heat release and the shock train; 3) provide preliminary design information, e.g., defining the isolator requirements and combustor area ratio as a function of initial conditions and level of heat release; and 4) provide engine performance estimates wherein the modeled processes τ_w, Q_w, and η_c are treated parametrically. Accordingly, some additional discussion of the integral method follows.

The conservation equations written in integral form for the general case depicted in Fig. 1 are given in Ref. 12. Evaluation of the shear on the combustor wall and Q_w rely on empirical correlations such as those given in Refs. 13 and 14. The experimental base for these correlations comprises 12 combustor geometries varying from 20–36 in. in length, numerous injector configurations, gaseous hydrogen and liquid fuels for combustors operating at simulated flight conditions of $M_0 = 4$–9. Scatter of the data is about ±20%. Although the form of the correlations was intentionally chosen to be general, i.e., normalized to the initial conditions, surface areas, driving enthalpies, etc., extrapolations to other initial conditions or extensions to different geometries would have to be validated. For well-designed combustors, wall shear and heat transfer must be kept small; consequently, the influence of deviation from the correlations is relatively small in the integral momentum and energy balances. Shear on the surfaces of the fuel injector is usually neglected, and the pressure distribution in the supersonic portion of this nozzle is taken either as isentropic throughout, or to the point where separation occurs. For high p_s/p_4 values, separation can occur, in which case the force is obtained assuming p_b acts on the affected area. Modeling for the wall force in the region of the shock train from 4 to s for simple axisymmetric configurations (Fig. 1) is presented in Ref. 15, and tests are currently being conducted at The Johns Hopkins University Applied Physics Laboratory to obtain data correlations for other configurations.[16] These tests will also either verify the presently used assumption $p_b = p_s$, or provide an alternate model. This leaves the evaluation of the integrals for the wall force from s to 5, to reduce the conservation equations to an algebraic form. This is accomplished by adopting a pressure area relationship, viz., $pA^{\varepsilon/\varepsilon-1} = C$ in the regions s to e and e to 5.

The so-called "ε = constant" model first suggested by Crocco[17] can be used in a variety of flowfield analyses. For simple flows, viz., constant area, constant pressure, or constant Mach number processes, wherein the one-dimensionality holds throughout, ε has prescribed constant values of 1, 0, or $-\gamma M^2$, respectively. Integral solutions do not, in general, require that the flow be unidimensional. Therefore, ε may be arbitrarily defined, determined from experiments, or can be a derived quantity from the solution of the equations. In this analysis ε_{s-e} is either assumed equal to ε_{e-5}, or is obtained from modeling of heat release rates in this zone. An explanation of the procedure is given in Ref. 7. The remaining integral in the momentum equation can be expressed as:

$$\int_{x_e}^{x_5} p \, dA_x = (1 - \varepsilon_{e-5})[p_5 A_5 - p_e A_e] \tag{1}$$

In solving the conservation equations in conjunction with the appropriate state equations, ε_{e-5} is not prescribed a priori, nor is the value of the pressure rise in the shock train p_s/p_4. Instead, the values of ε_{e-5} and p_s/p_4 are deduced by selecting the particular integral solution that not only satisfies the conservation equations but also meets the constraint $(\partial p/\partial A)_{\varepsilon=c} = (\partial p/\partial A)_{s=c}$, as $A \to A_5$ and $(dT_t/T_t) \to 0$ for a flow that is one-dimensional in the neighborhood of station 5. This simply states that the slope of the pressure area relationship for a constant ε process at the combustor exit, where the derivative of the total temperature approaches zero, should be equal to the slope of an isentropic process. More rigorously, the slope should match that of an adiabatic process that includes wall shear. However, if the shear terms are added, no simple analytic relationship has been found, and indeed, when typical experimental results are examined, the effects do not significantly affect this constraint.

With this constraint, the condition

$$M_5 = \left[\frac{\varepsilon_{e-5}}{\varepsilon_{e-5} + \gamma_5(1 - \varepsilon_{e-5})}\right]^{\frac{1}{2}} \tag{2a}$$

or

$$\varepsilon_{e-5} = \frac{\gamma_5 M_5^2}{1 + (\gamma_5 - 1)M_5^2} \tag{2b}$$

must be met, and a unique solution for each heat release can be obtained. That is, there is a specified shock train pressure rise for a given heat release. This result represents an analogous situation to the well-recognized choking point in Rayleigh heating and Fanno friction processes. Reference 18 gave the name "entropy limit" to solutions of the conservation equations that were so constrained. One caveat remains, viz., for the low area ratio combustors and high heat release rates, solutions to the equations would yield shock train pressure rises that would exceed that of a normal shock. For those cases, the slope

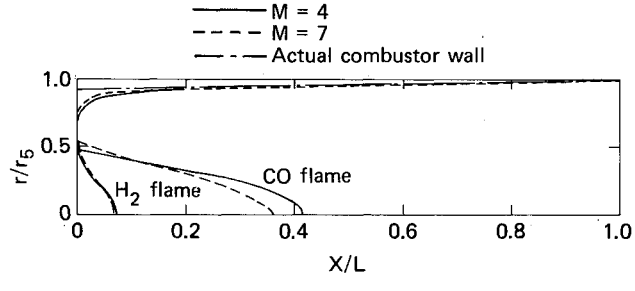

Fig. 3 Predicted duct contours and flame shapes for engine operating at Mach 4 and 7 with $ER = 0.5$.

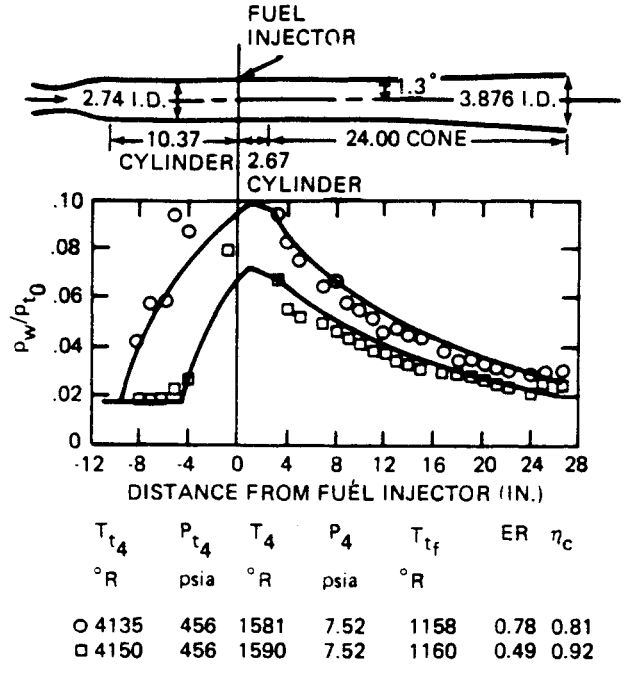

Fig. 4 Comparison of theoretical and experimental wall pressure distributions in a conical combustor at $M_4 = 3.23$.

constraint is relaxed, the normal shock pressure ratio is held, and the combustor exit Mach number M_5 is permitted to decrease. The limiting heat release for a combustor operating in this mode corresponds to $M_5 = 1$. Analysis of free-jet tests of scramjet engines verifies this mode of engine operation.

Figure 4 shows a typical result comparing experimental measurements with a solution of the integral equations. Wall pressure measurements from direct connect tests of a scramjet combustor are shown with the corresponding computed pressure distribution. For these tests at $M_4 = 3.23$, the η_c value used in the integral solution was determined from calorimetric measurements. More extensive comparisons of theory and experiment are presented in Ref. 7.

Simplified Solutions for Ideal Gases

The idealized case of a calorically perfect gas with $\gamma = 1.4$, which neglects wall shear and heat transfer and considers the mass and momentum contributions of the fuel to be negligible, can be used to explain the dependence of the shock train pressure rise on the amount of heat release. The explanation is more lucid if the additional simplifications $s_s - s_d = 0$, $p_e = p_s$, $\varepsilon_{s-e} = \varepsilon_{e-5} = \varepsilon$ are adopted.

Figure 5 shows a typical set of solutions for the case of $M_4 = 2.5$. The solid lines show the p_5/p_4 values as a function of the combustor area ratio for the entropy-limit solutions at selected shock train pressure ratios of 1, 2, 4, 6, and 7.125. The dashed curves for M_5 values of 1.0, 1.2, 1.4, 1.6, and 1.8 are solutions that correspond to the normal shock pressure rise $p_s/p_4 = 7.125$, but with the slope constraint at the combustor exit relaxed. Superposed on these solutions are curves corresponding to total temperature ratios of 1.5, 2, 3, 4, 5, and 6. For all $A_5/A_4 > 1$, $p_5 < p_s$.

The distinction between solutions resulting from this modeling and those for flows that are constrained to be unidimensional throughout is clearly evident for the particular case of $A_5/A_4 = 1$. As shown in Fig. 5, the $p_s/p_4 = 1$, 2, and 4 curves intersect the $A_5/A_4 = 1$ axis at $p_5/p_4 = 1$, 2, and 4, respectively. Upon closer examination it can be shown that for all values of $p_s/p_4 \leq 4.0625$, $p_5 = p_s$, whereas for all values of $p_s/p_4 > 4.0625$, there are no solutions at $A_5/A_4 = 1$. It can be rigorously proved that every combustor exit solution of $p_5/p_4 \leq 4.0625$ corresponds to an end-point state on the supersonic leg of a Rayleigh heating process, i.e., a one-dimensional frictionless heat addition process in a constant area duct. Moreover, the M_5 values are identical to those of the corresponding Rayleigh heating process. However, from Eq. (1) the slope constraint at station 5 requires $\varepsilon > 1$ for $M_5 > 1$. From a physical standpoint, this would imply that for all $T_{t_5}/T_{t_4} \leq 1.4083$, the value corresponding to $p_s/p_4 = 4.0625$, $M_5 = 1$, shock trains having strengths corresponding to single oblique waves would be present and not the shock-free, all-supersonic Rayleigh process. Note, too, that these results would also hold for cases where the shock train extends into the duct as long as wall friction is negligible. When wall friction is included, the same qualitative features are present, but the values of p_5/p_4 and p_s/p_4 shift for given values of T_{t_5}/T_{t_4}. Also, note that as A_5/A_4 is increased slightly above 1 in the wall-shear-free case, solutions for p_s/p_4 up to the normal shock value at M_4 are possible, but p_5/p_4 is always < 4.0625. This may also be seen in Fig. 6 where p_s/p_4, instead of p_5/p_4, is the ordinate.

Curves for constant T_{t_5}/T_{t_4} values from 1.1–2.6 are given in Fig. 6 as $f(A_5/A_4, p_s/p_4)$ for solutions constrained by the slope condition at the combustor exit. For values of $T_{t_5}/T_{t_4} \leq 1.4083$, the curves intersect the $A_5/A_4 = 1.0$ axis, and indeed there are valid solutions for $A_5/A_4 < 1$, i.e., for combustors with converging areas. The curves for $T_{t_5}/T_{t_4} > 1.4083$ are cusped at $A_5/A_4 \to 1$, i.e., there are also solutions for $A_5/A_4 < 1$, and those T_{t_5}/T_{t_4} curves also become asymptotic to the $A_5/A_4 = 1$ axis. Overlaid on this grid are dashed curves for constant M_5 values of 1.1–2.5 and the corresponding values of ε. The entropy-limit solutions for $p_s/p_4 = 7.125$ are limited to a maximum $T_{t_5}/T_{t_4} = 2.813$ for combustors with $A_5/A_4 \leq 4$.

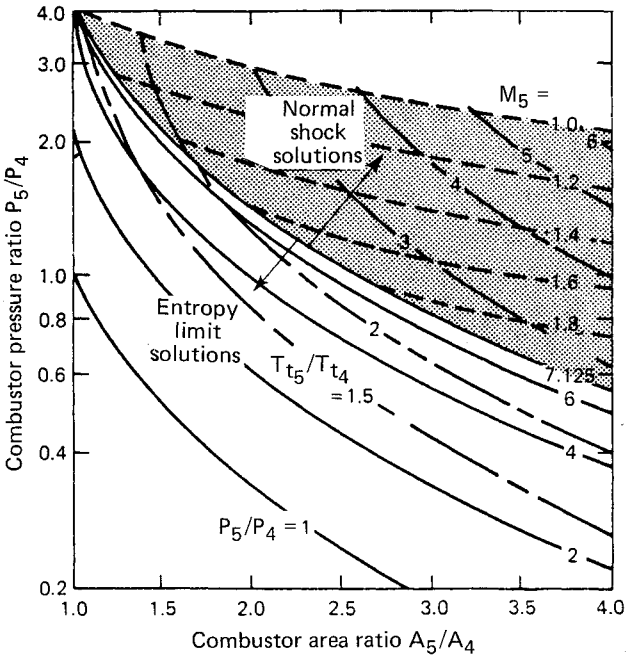

Fig. 5 Combustor exit pressure ratios for selected heat release rates ($M_4 = 2.50$, $\gamma = 1.4$, $\tau_w = 0$).

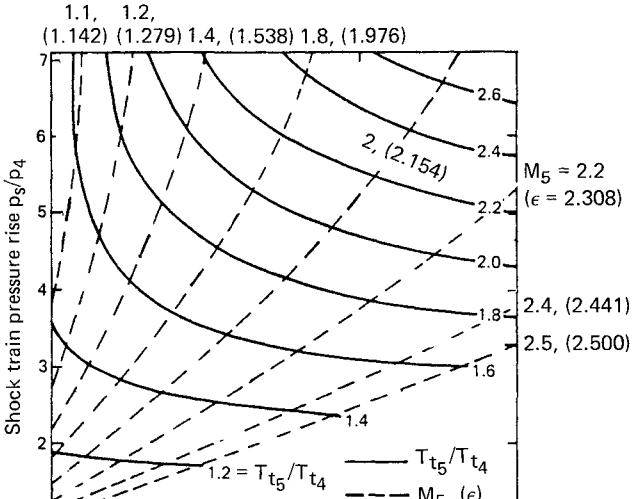

Fig. 6 Pressure ratios across precombustion shock train ($M_4 = 2.50$, $\gamma = 1.4$, $\tau_w = 0$).

However, if the exit slope condition is relaxed and M_5 is permitted to equal unity, the maximum T_{t_5}/T_{t_4} is 6.293 for $A_5/A_4 = 4$.

The rather abrupt increase in shock train pressure rise in low area ratio combustors with small increases in total temperature is depicted more clearly in Fig. 7. Curves of p_s/p_4 as $f(T_{t_5}/T_{t_4})$ for entropy-limit solutions are shown for selected values of A_5/A_4. For a combustor with $A_5/A_4 = 1.1$ and $M_4 = 2.5$, increasing T_{t_5}/T_{t_4} from 1.432–1.542, a mere 7.7%, doubles p_s/p_4 from 3.56 to 7.125. On the other hand, for large area ratio combustors, e.g., $A_5/A_4 = 4$, the shock pressure rise varies about linearly with T_{t_5}/T_{t_4}.

Solutions for a Transatmospheric Accelerator

Figure 8 shows the effect of combustor area ratio on the total pressure recovery in the heat-addition process. Curves for selected values of T_{t_5}/T_{t_4} between 1.1–3.0 are shown. Points above the dashed line correspond to entropy-limit solutions

and those below the dashed line are for shock trains with normal shock pressure ratios. Solutions are shown for M_5 values between 1–2.5. Entropy-limit solutions exist for $M_5 > 2.5$, but, as in Fig. 7, they are not included. Whereas larger values of A_5/A_4 can accommodate higher heat-release rates, there is an associated loss in total pressure recovery.

Additional assumptions, modeling, and definitions of engine size and operating conditions are needed to proceed with calculations for engine performance. Here, it is necessary to abandon the simplifying assumption of $\gamma = 1.4$, arbitrarily select a set of flight conditions, and use an appropriate equation of state throughout the engine cycle. In this exemplary case of a vehicle capable of flight from $M_0 = 3$–25, a trajectory having a constant dynamic pressure of $q_0 = 1000$ lb/ft^2 is adopted. Considerable attention must be given to the selection of a model for the inlet compression process. In previous studies, e.g., Ref. 7, empirical relationships between M_4/M_0 and kinetic energy efficiency, defined as

$$\eta_{KE} = \frac{h_{t_4} - h_4}{h_{t_0} - h_0} \tag{3}$$

were assumed. Whereas the modeling is adequate for the fixed-geometry engine studied therein, it would lead to anomalous operation for the variable-geometry inlet that would be required for a $M_0 = 3$–25 ramjet.

For a variable-geometry inlet, the inlet contraction ratio A_0/A_4 is adjusted within limits to provide a more optimal engine cycle. Examination of available test data and numerous inlet flowfield calculations suggest the following empirical relationship:

$$\frac{A_0}{A_4} = -3.7 + 2.3M_0 - 0.038M_0^2 \tag{4}$$

The corresponding inlet compression ratio p_4/p_0 is obtained from an empirical relationship for the mean Mach number, viz.,

$$M_4 = 0.43 + 0.38M_0 - 0.0051M_0^2 \tag{5}$$

Table 1 lists flow properties at stations 0 and 4 for selected values of M_0 for adiabatic compressions. The values of A_0/A_4 from Eq. (4) vary from 2.858 at $M_0 = 3$ to 30.05 at $M_0 = 25$, i.e., by a factor of 10.51. The required change in geometry would be significantly less for inlets that comprise external and internal compression due to inlet spillover. For example, if the spillover characteristics of the inlet were similar to that of a 5 deg half-angle conical inlet with shock-on-lip at $M_0 = 25$, the inlet capture ratio A_0/A_i would be 0.314 at $M_0 = 3$, thus, the required geometric variation would be reduced to $10.51 \times 0.314 = 3.30$. On the other hand, an all-internal contracting inlet would have to provide a full 10.51 to 1 area variation. Since A_0/A_i is dependent on the geometry of a particular engine, flight conditions, and angle of attack of the vehicle, rigorous solutions of the flowfield and/or testing is required for specification. Simple linear relationships, e.g.,

$$\frac{A_0}{A_i} = 1 - 0.1\left(8 - \frac{M_0}{3}\right) \tag{6}$$

can generally be used for preliminary design studies. Equation (6) would be approximate for the external-internal compression inlet in the exemplary case discussed herein for $3 \le M_0 \le 24$, and $A_0/A_i = 1$ for $M_0 > 24$. The pressure ahead of the shock train varies by less than a factor of two over the entire range in M_0. However, temperatures rise monotonically with M_0 reaching the level where dissociation would occur at $M_0 > 15$. The deduced values of η_{KE} show a minimum at $M_0 = 6$–7, and peak values at $M_0 = 20$. This somewhat irregular behavior in η_{KE} is the cause for difficulty in empirical modeling of η_{KE}. Although these calculations are for an inlet without heat losses—an atypical situation—the changes in p_4 and T_4 are quite small with heat loss. For example, at $M_0 = 20$ with a 1% loss in total enthalpy, i.e., 92 Btu/lb$_m$, p_4 decreases to 7.39 psia and T_4 decreases to 4742°R. The change in deduced η_{KE}, which is only an index and does not enter into the cycle calculation per se, is significant. With heat loss, η_{KE} drops to 0.9680 at this flight condition.

For the exemplary case, hydrogen fuel is injected tangentially ($\beta = 0$) with a total temperature of 2000°R at $M_f^* = M_b = 1$, and $p_f^* = p_b = p_4$. Combustor shear was modeled at $C_f A_w/A_4 = 0.02 = \tau_w/q_4 A_4$ and, as before, $S_s = S_d$; $\varepsilon_{s-e} = \varepsilon_{e-5}$. Results of the combustor calculations are summarized in Fig. 9. Combustor-inlet Mach number is the linear

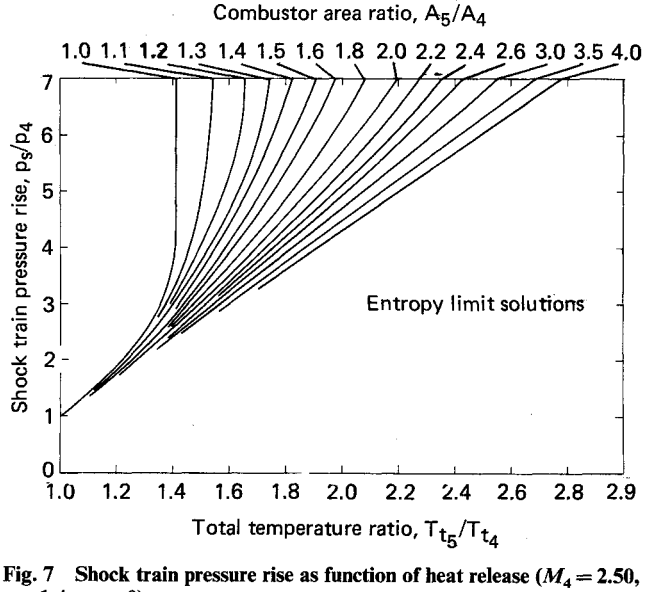

Fig. 7 Shock train pressure rise as function of heat release ($M_4 = 2.50$, $\gamma = 1.4$, $\tau_w = 0$).

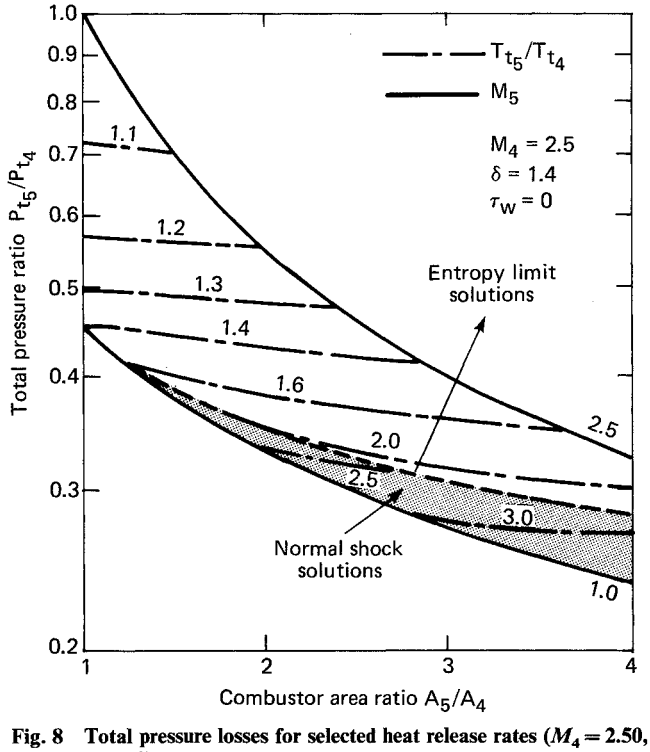

Fig. 8 Total pressure losses for selected heat release rates ($M_4 = 2.50$, $\gamma = 1.4$, $\tau_w = 0$).

Table 1 Conditions in freestream and combustor inlet for adiabatic compression ($q_0 = 1000$ lb/ft^2)

	Freesteam conditions			Combustor inlet conditions				
M_0	Z_0, KFT	P_0, psia	T_0, °R	M_4	A_0/A_4	P_4, psia	T_4, °R	η_{KE}
3	59.0	1.102	390.0	1.524	2.858	8.67	752	0.9637
4	71.0	6.200^{-1}	392.8	1.868	4.892	10.38	980	0.9624
5	80.5	3.968^{-1}	398.0	2.203	6.850	11.01	1224	0.9578
6	88.4	2.756^{-1}	402.2	2.526	8.732	11.15	1467	0.9570
7	95.1	2.025^{-1}	405.9	2.840	10.538	11.07	1705	0.9585
10	110.9	9.921^{-2}	419.7	3.720	15.500	10.20	2408	0.9656
15	129.9	4.409^{-2}	448.5	4.983	22.250	8.74	3617	0.9738
20	144.1	2.480^{-2}	470.1	5.990	27.100	7.56	4824	0.9762
25	155.7	1.587^{-2}	487.2	6.743	30.050	6.55	5822	0.9719

scale on the abscissa which, from Eq. (5), leads to the nonlinear M_0 scale that is also shown. The solid curves for A_5/A_4, p_s/p_4, and p_s correspond to the minimum possible area ratio combustor for the respective ER and M_4, i.e., $M_5 = 1$. Minimum combustor area ratios decrease rapidly from 2.09 to $ER = 0.25$ and 4.10 at $ER = 1$ for $M_4 = 1.524$ ($M_0 = 3$) to $A_5/A_4 = 1$ at $M_4 = 2.34$ ($M_0 = 5.42$) for $ER = 0.25$ and $M_4 = 3.00$($M_0 = 7.52$) for $ER = 1$. For all of these processes, the shock train pressure rise is equivalent to a normal shock that leads to the increasing p_s/p_4 values and p_s levels as M_0 increases on a constant-q_0 trajectory. All of these solutions also have $M_5 = 1$. Once the $A_5/A_4 = 1$ condition is reached, the shock train pressure rises correspond to equivalent oblique-shock compressions that weaken rapidly with increasing M_0. All of these solutions are at the respective "entropy limits." Performance at high M_0 would decrease to unacceptably low values if A_5/A_4 were permitted to go much above 1. Thus, from Fig. 9a it is apparent that a combustor designed to operate over the entire M_0 range would require variable A_5/A_4. Moreover, A_4 must vary, thus, variable geometry is needed. However, the amount of geometric variation can be significantly reduced by a combustor design that comprises a constant-area section followed by a divergent section. At high M_0, fuel is injected in the upstream end of the constant-area section, and sufficient length is provided to add all of the heat prior to entering the divergent section. At low M_0, some fuel is injected in the constant-area section, and the remainder is injected in the divergent portion. Note, however, that at low M_0 the amount of heat that can be added in the constant-area section is quite small, as evidenced by the $ER = 0.25$ curve in Fig. 9a. In fact, at $M_0 = 4$ ($M_4 = 1.87$) the maximum ER to prevent choking in the constant-area section is 0.059.

Although the minimum A_5/A_4 yields the maximum engine performance, it may not lead to the optimal design, since the combustor structure would have to be designed to withstand the maximum p_s. Moreover, the corresponding maximum value of p_s/p_4 could lead to excessive isolator requirements to avoid combustor-inlet interactions. Consequently, a better overall design strategy may be to limit the maximum p_s and accept somewhat lower performance. The dashed curves in Fig. 9 correspond to such a design approach wherein p_s is limited to 50 psia. For clarity, only the $ER = 0.5$ curves are shown. To reduce p_s to 50 psia at $ER = 0.5$ would require the increase in A_5/A_4 shown in Fig. 9a. All of these solutions would correspond to entropy-limit cases with $M_5 > 1$. Increasing A_5/A_4 at a given ER has very little effect on engine specific impulse because the increased loss in total pressure in the combustor is compensated by a corresponding decreased loss in the precombustion shock train. This was also evident in the $\gamma = 1.4$ results as indicated by the nearly constant values of p_{t_5}/p_{t_4} shown in Fig. 8 for constant values of T_{t_5}/T_{t_4} near the entropy limit.

Reducing ER is the only practical method for reducing p_s at low M_0. For example, at $M_0 = 5$, to lower p_s from the normal shock value of 59.9 psia to 50 psia, but maintaining $ER = 1$,

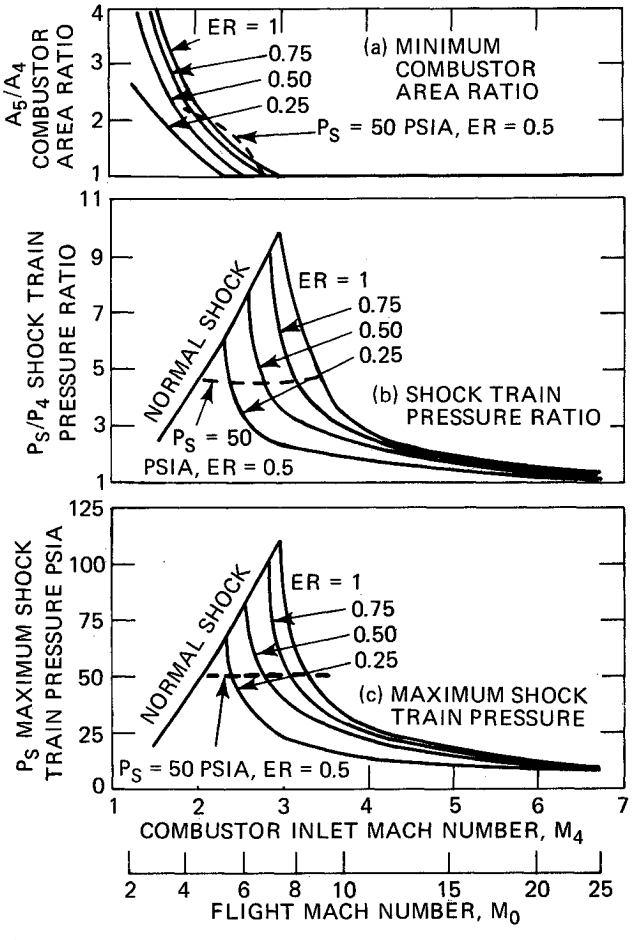

Fig. 9 Combustor geometry and shock train pressure rise ($q_0 = 1000$ lb$_f$/ft^2).

would require an increase in A_5/A_4 from 1.85 to 12.0. By reducing ER, the A_5/A_4 values that correspond to ER's of 0.75, 0.50, and 0.25 are 5.48, 2.48, and 1.28, respectively.

The large changes in p_s that result from small changes in A_5/A_4 for near-constant-area combustors suggest that considerable attention must be paid to engine control. Fortunately, the pressure can be measured accurately, and the required dynamic range of less than a factor of 10 for the constant-q_0 trajectory is well within the capability of most sensors. On the other hand, to obtain the desired A_5/A_4 will require extremely clever concepts for staged fuel injection.

More extensive discussion of the application of the integral technique for the estimation of engine performance and evaluation of experimental results are given in Refs. 7 and 13.

Planar Heat Release

The concept of an oblique planar heater (OPH) as a method for modeling heat release in supersonic flow is more readily understood with the help of Fig. 10. An OPH is defined as an infinitesimally thin planar flame front in which heat is added and the velocity vector is changed. In principle, both the "weak" OPH, in which the planar heater angle θ, with respect to the upstream velocity vector u_1, is less than the upstream Mach angle $\mu = \text{arc sin}(1/M_1)$, and the "strong" OPH ($\theta > \mu$), are conceptually possible. For the weak OPH, u_{1N} is subsonic and u_{2N} is either subsonic or sonic. For the strong OPH, u_{1N} is supersonic, a positive turning of the flow (counterclockwise in Fig. 10) is required, and u_{2N} is either supersonic or sonic. To avoid a converging combustor, the strong OPH must be coupled with a centered isentropic expansion or a weak OPH, or with some combination of the two. Converging combustors are not presented in this paper because the maximum engine contraction ratio has been governed by the inlet, i.e., by A_0/A_4, not A_0/A_5 for which it can be shown leads to higher engine performance.

For an ideal gas, the following governing equations hold for the OPH:

$$\tan(\theta + \delta) = (1 + \gamma M_1^2 \sin^2\theta)/(1 + \gamma) M_1^2 \sin\theta \cos\theta \quad (7)$$

$$p_2/p_1 = (1 + \gamma M_1^2 \sin^2\theta)/[1 + \gamma M_2^2 \sin^2(\theta + \delta)] \quad (8)$$

and

$$T_2/T_1 = (p_2/p_1)^2 M_2^2 \sin^2(\theta + \delta)/M_1^2 \sin^2\theta \quad (9)$$

where the p's and T's are static pressures and temperatures upstream (subscript 1) and downstream (subscript 2) of the OPH. In this discussion, the further restriction of the so-called "oblique Chapman-Jouget condition"[19] will also be met, i.e., the normal component of the Mach number downstream of the OPH [$M_2 \sin(\theta + \delta)$] will be set equal to one.

If the question of the practicality of the mechanism for injecting and mixing fuel in such a manner to instantaneously react along a planar surface (often referred to as a "flame sheet") is begged, then interesting combinations of weak OPH's and oblique waves can be constructed, all rigorously satisfying the conservation equations. Figure 11 shows four models, each of which returns the velocity vector to its initial direction in the combustor-exit plane.

The wave structures and wall shapes for all cases correspond to solutions for total temperature ratios $T_{t5}/T_{t4} = 1.3$ with $M_4 = 2.5$ and $\gamma = 1.4$, in order that direct comparisons can be made with the results shown in Figs. 6–8. The height of the duct at station 4 was selected to permit the sketches to be about the same overall size. Had they all been drawn for the same A_4, cases b and d would be relatively much smaller. In Fig. 11a, the first weak OPH turns the flow 10.82 deg ($\theta = 12.92$ deg) away from the axis; then, at the point where the weak OPH strikes the axis, a second weak OPH returns the flow to its initial direction. In Fig. 11b, an oblique shock turns the flow 17.46 deg away from the axis and a weak OPH emanating from the same point on the axis turns the flow parallel to the lower surface. This model is particularly interesting for two reasons. It closely approximates the integral model, and, in fact, solutions for the two models differ only by the small change in wall force. Moreover, when the precombustion shock reaches its maximum strength ($\delta_w \to 0$, $\theta_w \to 90$ deg), the model is equivalent to a standing normal detonation wave. In Fig. 11c, a weak OPH emanating from the top wall turns the flow 15.66 deg ($\theta = 10.26$ deg) outboard. The point where this weak OPH strikes the axis serves as the focal point of a Prandtl-Meyer expansion that turns the flow back through the 15.66 deg. Figure 11d shows a strong OPH ($\delta = 10.24$ deg, $\theta = 63.91$ deg), followed by a centered Prandtl-Meyer expansion emanating from the same point on the axis. For all cases, the geometry and wave structure would change for different values of M_4 or T_{t5}/T_{t4}.

Figure 12 summarizes results for the four types of processes as a function of T_{t5}/T_{t4} for $M_4 = 2.5$. The weak OPH followed by the isentropic expansion ($s = c$) process (case c) requires the largest A_5/A_4 that leads to the lowest p_5/p_4 for a given T_{t5}/T_{t4}. The double OPH process (case a) requires about 65% of the A_5/A_4 of case c and has a correspondingly higher p_5/p_4. All solutions for the other two cases turn out to be close to constant-area processes. The two branches of solutions for case b correspond to the weak and strong solutions for the oblique shock, and in the limit of a normal shock, the solutions for cases c and d coincide. Whereas solutions exist for arbitrarily large values of T_{t5}/T_{t4} for a and c, cases b and d have maximum possible heat release rates. For cases b, the maximum value of $T_{t5}/T_{t4} = 1.71$ corresponds to the maximum turning angle of the oblique shock, viz., $\delta_w = 29.80$ deg, $\theta_w = 64.78$ deg for $M_4 = 2.5$. For $\theta_w > 62.65$ deg, the Mach number behind the shock is subsonic.

The turning angles shown for case a are the sums of the two OPH's which, for a given T_{t5}/T_{t4}, exceeds the turning in any of the other models. For cases b, c, and d, the turning angles shown do not include either the shock or the isentropic turn. Solutions for case d show that there is a maximum turning angle for strong OPH's, $\delta = 10.76$ deg, $\theta = 56.85$ deg for $M_4 = 2.5$, which is analogous to the maximum turning for oblique shocks. The near constant area processes (cases b and

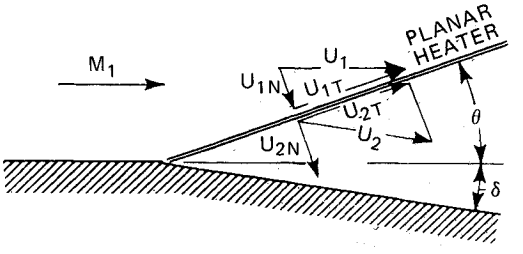

Fig. 10 Schematic illustration of an oblique planar heater.

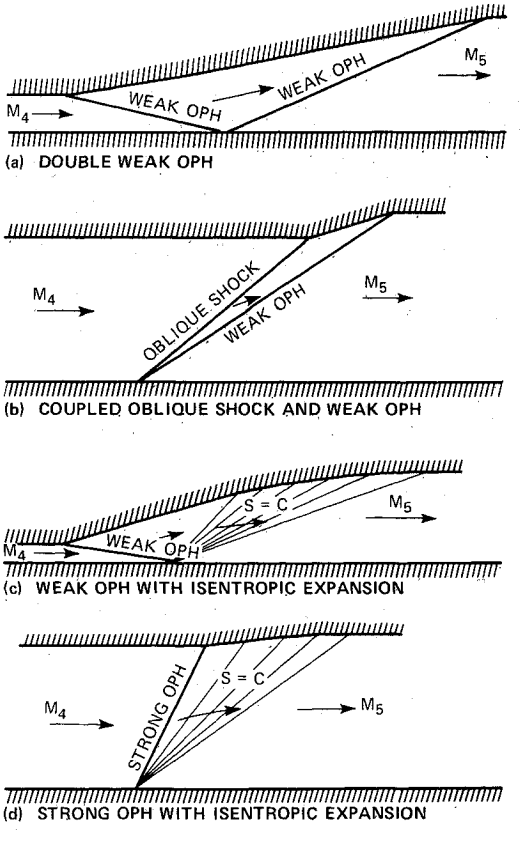

Fig. 11 Schematic illustrations of planar flame models.

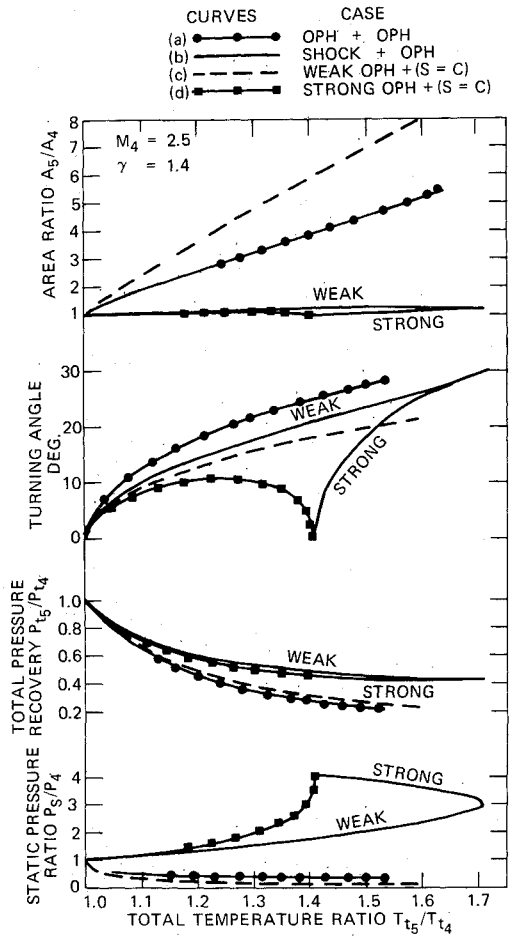

Fig. 12 Properties of combustors with oblique planar heaters.

d) have the highest total pressure ratios, p_{t_5}/p_{t_4}, for a given T_{t_5}/T_{t_4}, with the weak shock solutions for case c having the highest values. The values of p_{t_5}/p_{t_4} for the "weak" shock leg of case b are about the same as those shown in Fig. 8 for the integral model for $T_{t_5}/T_{t_4} < 1.2$. For higher values of T_{t_5}/T_{t_4}, the p_{t_5}/p_{t_4} values for case c are about 5–10% higher. Note that for values of $T_{t_5}/T_{t_4} > 1.71$, the models for the integral analysis would have higher p_{t_5}/p_{t_4} than those for cases a and c.

Concluding Remarks

The capability of the coupled integral and finite-difference solution to describe many of the flow properties in supersonic diabatic flow lies in the judicious selection of boundary conditions. This is not atypical of many problems in fluid mechanics. Complex internal flows are generally characterized by regions of separated flow that are difficult to define accurately. Consequently, techniques, such as used herein, which suppress the dependence of the solution on an accurate definition of the separated zone can enjoy considerable success.

Physical situations wherein the planar flame models would be closely approximated are difficult to postulate. Nevertheless, the variety of combinations of shocks and OPH's provides considerable insight into the interplay of shocks, expansions, and heat addition.

References

[1]Shapiro, A. H., *The Dynamics and Thermodynamics of Compressible Fluid Flow*, Vol. 1, Ronald Press, New York, 1953, pp. 219–260.

[2]Kumar, A., "Numerical Simulation of the Flow Through Scramjet Inlets Using a Three-Dimensional Navier-Stokes Code," AIAA Paper 85-1664, July 1985.

[3]Chu, B.-T., "Pressure Waves Generated by Addition of Heat in a Gaseous Medium," NACA TN-3411, June 1955.

[4]Tsien, H. S. and Beilock, M., "Heat Source in a Uniform Flow," *Journal of the Aeronautical Sciences*, Vol. 16, Dec. 1949.

[5]Billig, F. S., "Two-Dimensional Model for Thermal Compression," *Journal of Spacecraft and Rockets*, Vol. 9, Sept. 1972, pp. 702–703.

[6]Ferri, A., "Review of SCRAMJET Propulsion Technology," *Journal of Aircraft*, Vol. 5, Jan.–Feb. 1968, pp. 3–10.

[7]Billig, F. S., "Ramjets with Supersonic Combustion," AGARD-NATO PEP Lecture, Series No. 136, Ramjet and Ramrocket Propulsion Systems for Missiles, Sept. 1984.

[8]Billig, F. S., Waltrup, P. J., and Stockbridge, R. D., "Integral-Rocket Dual-Combustion Ramjets: A New Propulsion Concept," *Journal of Spacecraft and Rockets*, Vol. 17, Sept.–Oct. 1980, p. 416.

[9]Kumar, A., "Numerical Analysis of the Scramjet-Inlet by Using Two-Dimensional Navier-Stokes Equations," NASA TP-1940, Dec. 1981.

[10]Schetz, J. A., Billig, F. S., and Favin, S., "Flowfield Analysis of a Scramjet Combustor with a Coaxial Fuel Jet," *AIAA Journal*, Vol. 20, Sept. 1982, pp. 1268–1274.

[11]Griffin, M. D., Billig, F. S., and White, M. E., "Applications of Computational Techniques in the Design of Ramjet Engines," 6th International Symposium on Air Breathing Engines, Paris, France, June 1983.

[12]Billig, F. S., "Combustion Processes in Supersonic Flow," 7th ISABE Beijing, People's Republic of China, Sept. 1985, pp. 245–256.

[13]Billig, F. S., Orth, R. C., and Funk, J. A., "Direct-Connect Tests of a Hydrogen-Fueled Supersonic Combustor," NASA-CR-1904, Aug. 1971.

[14]Billig, F. S. and Grenleski, S. E., "Heat Transfer in Supersonic Combustion Processes," Fourth International Heat Transfer Conference, Versailles, France, Aug. 1971.

[15]Waltrup. P. J. and Billig, F. S., "The Structure of Shock Waves in Cylindrical Ducts," *AIAA Journal*, Vol. 2, Oct. 1973, pp. 1404–1408.

[16]Stockbridge, R. D., "A Computational Method for Determining Flowfield Properties in an Internal Supersonic Turbulent Axisymmetric Flowfield When the Pitot Pressure is the Only Measured Instream Property," Presented at the 8th International Symposium on Air Breathing Engines, Cincinnati, OH, June 1987.

[17]Crocco, L., "One Dimensional Treatment of Steady Gas Dynamic," *Fundamentals of Gas Dynamics*, High Speed Aerodynamics and Jet Propulsion, Vol. 3, Princeton University Press, Princeton, NJ, 1958, pp. 105–130.

[18]Billig, F. S., "Design of Supersonic Combustors Based on Pressure-Area Fields," *Eleventh Symposium (International) on Combustion*, The Combustion Institute, Pittsburgh, PA, 1967, pp. 755–569.

[19]Billig, F. S., "External Burning in Supersonic Streams," Applied Physics Lab., The Johns Hopkins Univ., Silver Spring, MD, TG 912, May 1967.